Automated Interpretation of Planar Thallium-201-Dipyridamole Stress-Redistribution Scintigrams Using Artificial Neural Networks

Gerold Porenta, Georg Dorffner, Stephan Kundrat, Paolo Petta, Johanna Duit-Schedlmayer and Heinz Sochor

Department of Cardiology, 2nd Clinic of Internal Medicine and Department of Medical Cybernetics and Artificial Intelligence, University of Vienna Medical School; and Austrian Research Institute for Artificial Intelligence, Vienna, Austria

To develop an automated image interpretation system of planar cardiac ^{201}Tl dipyridamole stress/redistribution scintigrams, the authors used artificial neural networks that associate patterns of segmental myocardial thallium uptake with a diagnostic assessment about the presence, severity and localization of significant coronary artery disease. **Methods:** Artificial neural networks were trained and evaluated using the results from segmental thallium analysis and either expert readings in 159 cases or coronary angiography in a subgroup of 81 patients. **Results:** Based on receiver operating characteristics analysis, the sensitivity for the detection of significant coronary artery disease at a specificity of 90% was 51% compared with angiography and 72% compared with the human expert. For severity and localization of disease, two vascular territories assigned to the vascular bed of the left anterior descending (LAD) artery and to the territory subtended by the left circumflex artery and the right coronary artery together (CX/RCA) were included in the analysis. **Conclusion:** Artificial neural networks may be useful to develop automated computer-based image interpretation systems of ^{201}Tl perfusion scintigrams. However, utilization of large training datasets appears to be a prerequisite to achieve adequate diagnostic performance.

Key Words: myocardial scintigraphy; thallium-201; dipyridamole; artificial neural networks; receiver operating characteristics analysis

J Nucl Med 1994; 35:2041–2047

Planar ^{201}Tl-dipyridamole stress/redistribution perfusion scintigraphy is frequently used in the evaluation of patients with suspected or proven coronary artery disease (CAD) (*1–3*). Clinical applications include the detection of significant CAD and the assessment of its severity and localization. In addition, valuable prognostic information for patient management can also be obtained from planar thallium scintigrams (*4,5*).

Received Nov. 16, 1993; revision accepted May 5, 1994.

For correspondence or reprints contact: Gerold Porenta, MD, PhD, Department of Cardiology, 2nd Clinic of Internal Medicine, University of Vienna Medical School, Währinger Gürtel 18-20, A 1090 Vienna, Austria.

Although visual interpretation of raw images was initially used for image analysis, semiquantitative methods, including circumferential profile analysis with the possibility of comparing patient data to a reference normal database, were subsequently introduced to decrease intra- and interobserver variability and improve the diagnostic accuracy of planar thallium imaging (*6–9*).

In recent years, research in artificial intelligence has developed computer methods that permit the building of automated diagnostic systems with the capability of knowledge representation and machine learning (*10*). Rule-based expert systems and artificial neural networks have emerged as powerful tools to construct computer programs that attempt to solve problems that traditionally required human expertise. Compared with rule-based systems, artificial neural networks offer the advantage of intrinsic incremental knowledge acquisition with the capability of learning from case examples and thus appear to be particularly suited for image analysis and interpretation.

Several earlier studies have utilized artificial intelligence techniques in an attempt to advance from computer-based image processing to computer-based image interpretation and have created computer programs for an automated interpretation of ^{201}Tl scintigrams (*11–15*). However, although these initial approaches appeared promising, their clinical utility and diagnostic accuracy remained undetermined.

The purpose of the present study was to (1) develop artificial neural networks that automatically detect the presence of CAD and assess its severity and localization based on the segmental analysis of planar thallium stress/redistribution scintigrams and (2) evaluate their diagnostic accuracy in comparison with coronary angiography and human expert interpretation.

METHODS

Study Population

The study population was compiled by a retrospective database search and included 159 patients (120 males and 39 females; age 56 ± 9 yr mean ± s.d.; range 33–74 yr) who had undergone planar dipyridamole stress/redistribution ^{201}Tl scintigraphy at the cardio-

vascular nuclear medicine laboratory of this department. Forty-four (28%) patients had suffered at least one prior transmural myocardial infarction.

In a subgroup of 81 patients, coronary angiography was performed using the Judkins technique within 6 mo of the thallium study to confirm or exclude significant CAD and to assist in patient management. The clinical course of patients between angiography and thallium scintigraphy was uneventful. In particular, there was no indication of an intercedent myocardial infarction or any other sign of progressive coronary artery disease.

Angiograms were reviewed by experienced staff cardiologists who were not specifically blinded to the thallium results. In 67 of 81 patients, angiography revealed significant CAD, defined as 50% or more luminal diameter narrowing in at least one major epicardial coronary artery. To facilitate a comparison between the severity of CAD, defined by angiography and by thallium scintigraphy, the total myocardial perfusion bed was divided into two vascular territories. One territory was assigned to the vascular bed of the left anterior descending (LAD) artery; the other territory was assigned to the vascular bed subtended by the circumflex artery (CX) and the right coronary artery (RCA). This particular distinction was adopted for two reasons. First, planar thallium scintigraphy, in contrast to SPECT imaging, has been shown to have a low sensitivity for the detection of disease in the individual vascular territories of the CX and RCA (*16*). Second, the origin of the posterior descending artery and the posterolateral arterial branches varies between the CX and the RCA, so that the amount of myocardial tissue supplied by either vessel is variable. Thus, for the purpose of the present study, the severity of CAD was classified into single- or multiple-territory disease.

According to this classification, 34 (42%) patients had evidence of significant CAD in only one territory (21 LAD and 13 CX and/or RCA). In 33 (41%) patients, both territories were affected. In 14 (17%) patients, coronary angiography did not reveal significant CAD. Patients who had previously undergone angioplasty or coronary artery bypass surgery were excluded from the angiography subgroup of our study.

Thallium Image Acquisition and Analysis

Patients were injected with dipyridamole (0.67 mg/kg) over a period of 4 min. If the heart rate response to pharmacologic stress was insufficient to increase the resting heart rate by at least 10%, an isometric hand-grip exercise was performed. Following the application of the vasodilating agent, 74 to 111 MBq (2–3 mCi) of ^{201}Tl was injected intravenously, and multiple-view images were acquired for 8 min in three standard projections (anterior, left anterior oblique [LAO] 45° and LAO 70°) with a planar gamma camera (Apex 215, LEAP collimator, Elscint Co., Boston, MA). The same image projections were then repeated after 3 to 4 hr with the patient at rest. A sample set of images is depicted in Figure 1.

Quantitative segmental thallium analysis was performed based on circumferential profile analysis using a commercially available computer program (CTLSEG, Elscint Co.). Briefly, after background substraction and smoothing, circumferential profiles of maximal count activity were generated with the use of radii spaced apart by 6°. The profiles were aligned with the apex at 180° according to operator specification. Normalized segmental values were then computed for five 60° segments in each view. The sixth 60° segment was considered the valve segment and omitted from further analysis. For each segment, a washout index was computed. In total, a single dataset consisted of 45 integer numbers that reflected the relative segmental thallium uptake at stress and

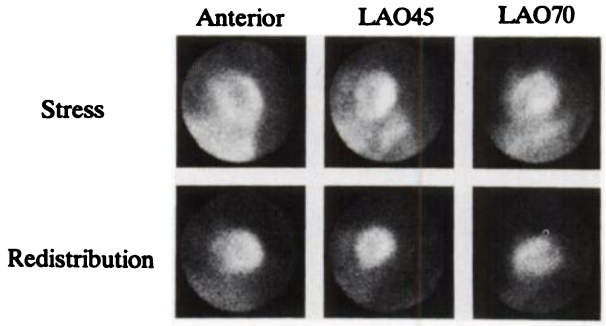

FIGURE 1. Sample set of planar thallium dipyridamole stress/redistribution images with three standard views obtained in a patient evaluated for CAD. Perfusion scintigraphy shows significant redistribution in the anterior wall.

after redistribution and the relative segmental washout in five myocardial segments in each of the three standard views. A sample dataset of the segmental thallium analysis for the thallium study depicted in Figure 1 is given in Table 1. These values of segmental thallium uptake and washout served as the input dataset for image interpretation by artificial neural networks.

All thallium studies (n = 159) were graded independently for the presence, severity and localization of coronary artery disease by one experienced human observer (H.S.) who used scoring schemes with nominal scale gradations. For binary yes/no decisions, a grading of equivocal was possible, but these cases were not used for training and evaluation of neural networks. For the

TABLE 1
Sample Report of Segmental Values for Myocardial Thallium Uptake and Washout Obtained from the Images Depicted in Figure 1*

Scintigraphic Views	Stage	Myocardial Segments					
		Ant-Lat		Apex	Inf		
Ant	Stress	96	94	74	83	73	
	Redistribution	94	86	79	86	79	
	Washout	59	61	54	57	54	
		Post-Lat		Apex	Septum		
LAO 45	Stress	49	67	87	88	54	
	Redistribution	75	77	86	98	71	
	Washout	54	65	71	67	60	
		Post-Inf		Apex	Ant-Sept		
LAO 70	Stress	63	95	83	38	25	
	Redistribution	90	98	76	53	53	
	Washout	55	69	73	58	36	

*Forty-five integer values as in this example were used as an input pattern for the artificial neural networks.

Scintigraphic views: Ant = anterior; LAO 45 = left anterior oblique 45°; LAO 70 = left anterior oblique 70°.

Myocardial segments: Ant-Lat = anterolateral; Ant-Sept = anteroseptal; Post-Lat = posterolateral; Post = posterior; Inf = inferior; Apex = apical.

presence of significant CAD, 53 (33%) studies were graded as normal; 88 (56%), as abnormal; and 18 (11%), as equivocal. For severity of disease, 46 (29%) studies were classified as single-territory disease; 58 (36%), as double-territory disease; and 55 (35%), as normal. For localization of disease, the territory assigned to the LAD artery was read as normal in 66 (42%) studies, as abnormal in 75 (47%) and as equivocal in 18 (11%). The territory assigned to the left CX and RCA was called normal in 59 (37%), abnormal in 78 (49%) and equivocal in 22 (14%) cases. In one case, both territories were graded as equivocal.

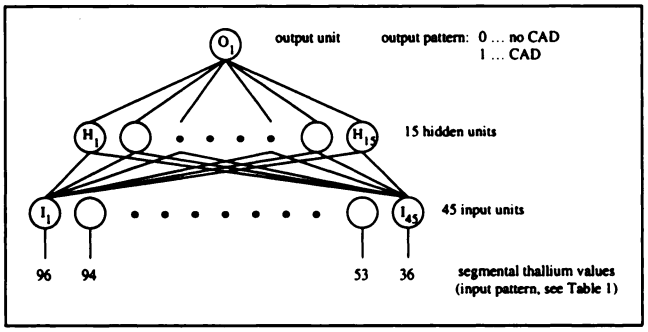

FIGURE 2. Schematic diagram of an artificial neural network designed to associate segmental values of myocardial thallium uptake and washout as input pattern with an output pattern concerning the presence of significant CAD.

Artificial Neural Networks

Applications of artificial neural networks have been described and reviewed in detail elsewhere (*17–19*). Briefly, artificial neural networks consist of simple computing units that are connected in a specific network topology, commonly a three-layered structure, i.e., an input layer, an output layer and a hidden layer that mediates all connections between the input and output units. Input patterns are encoded as activation patterns of the input units; the state of the output units is decoded into an output pattern. For each unit, a nonlinear transfer function computes from its input values a unique and usually binary output value encoded as 0 or 1. Weight factors that are associated with each interunit connection are multiplied with output values to yield scaled input values for the connected units.

Artificial neural networks for pattern recognition can be developed utilizing heuristic rules and learning algorithms that operate on training sets of characteristic case examples. First, the topology and the hierarchy of the network have to be specified based on the problem specification and on adequate coding schemes of input and output patterns. Frequently, empiric strategies have to be applied to assign units to each network layer because algorithms that would precisely predict the optimal network configuration based on a specific problem specification are, in general, not available. Then, numeric weight factors are determined for each unit-to-unit connection by an iterative learning algorithm. After random initialization of the weight matrix, the first input pattern of the training set is processed by the network to generate the associated output pattern. The difference between the observed and the expected output pattern is used to adjust the weight matrix appropriately utilizing the backpropagation algorithm (*17*). Additional iterations for the same pair of input-output patterns continue until the network correctly derives the expected output pattern. Sequentially, all remaining patterns of the training set undergo the same procedure. To ascertain adequate diagnostic performance of the network also for patterns that are not specifically included in the training set, the training set should include a representative sample of cases from the entire problem domain.

Specific Network Design. Artificial neural networks used in the present study consisted of 45 input units, 15 hidden units, and 1 or 2 output units to determine the presence, severity and localization of CAD. Each of the 45 input units was assigned to a corresponding input value of the segmental thallium analysis. Although the number of the input and output units was determined by the structure of the input and output patterns, the number of hidden units was chosen empirically as 15, an intermediate level between the number of input and output units. Initial tests in which the number of hidden units was varied indicated that the performance of the network was insensitive to small variations in the number of hidden units. A schematic diagram of the adopted network topology for the detection of CAD is given in Figure 2. Different network instances were developed to predict the results from either angiography or human image interpretation.

From the entire database, subsets of cases were selected as training sets; the remaining cases were used to evaluate the performance of the network. Although a large training set would be desirable to improve network performance, cases that are assigned to the training dataset cannot be used to evaluate the diagnostic accuracy of the network. Therefore, the fraction of cases that was included in the training data set was chosen empirically as 20% to 30% so that an adequate number of cases could be assigned to the training set and the evaluation set. To ensure an adequate case representation within training sets and at the same time achieve statistical independence between sets, the case distribution in the training sets was constrained to reflect proportionally the distribution of cases in the entire database with the additional requirement of a minimal overlap between training sets. Table 2 summarizes the distribution of patterns selected for the training sets.

An alternative approach to develop and evaluate artificial networks with a database of n cases would involve the generation of n different network instances by partitioning the total number of cases into a training set of $n - 1$ cases and an evaluation set of 1 case for all n possible permutations. However, this "round robin" method does not result in the development of one specific network instance that can be evaluated in a separate evaluation step but rather generates n different network instances that are statistically not independent. Moreover, analysis software that would permit the generation of receiver operating characteristics (ROC) curves, as indicated later, also for data obtained by this approach was not available. Therefore, this method was not applied in the present study.

Network training was conducted based on the backpropagation algorithm with a learning rate of 0.1, a scaling factor of the momentum term of 0.9 and a threshold at the output unit of 0.3. The computer experiments were performed on an Apollo DN3000 UNIX workstation (Hewlett Packard, Palo Alto, CA) using computer software written in C and the network simulation language VieNet2 for neural network simulation (*20*).

Analysis of Network Performance. Neural networks were developed to provide diagnostic information on three different aspects of CAD with appropriately designed output patterns. The presence of significant CAD was associated with a simple binary output pattern (yes/no). The severity of disease was assessed based on a classification into three mutually exclusive categories (normal, single territory or multiple territory), and the localization

TABLE 2
Case Distribution Between Subsets Used for Training and Evaluation of Artificial Neural Networks Developed to Interpret Thallium Data According to Presence, Severity and Location of Significant CAD*

	Training Set	Evaluation Set	Total Database
Presence of CAD			
Angiography			
Normal	5	9	14
Abnormal	15	52	67
Human expert			
Normal	15	38	53
Abnormal	15	73	88
Equivocal			18
Severity of CAD			
Angiography			
Normal	4	10	14
Single territory	12	22	34
Multiple territory	12	21	33
Human expert			
Normal	12	43	55
Single territory	10	36	46
Multiple territory	13	45	58
Location of CAD			
Angiography			
Normal	4	10	14
LAD alone	6	15	21
CX/RCA alone	4	9	13
Both territories	6	27	33
Human expert			
Normal	8	33	41
LAD alone	4	9	13
CX/RCA alone	6	11	17
Both territories	8	41	49
Equivocal			39

*Results from coronary angiography (n = 81) and human expert readings (n = 159) were used as reference standards.

LAD = vascular territory subtended by the left anterior descending artery; CX/RCA = vascular territory subtended by the left circumflex and right coronary artery.

of disease was encoded by two mutually not exclusive binary decisions for the presence of disease in each of the two vascular territories (LAD: yes/no, CX/RCA: yes/no). According to the output patterns for each network topology, different approaches were used to analyze network performance.

For the detection of CAD, ROC curves (*21*) were derived for each of the five network instances by comparing the output data obtained during network evaluation with the results from angiography and with human expert readings. For diagnostic tests that are designed to differentiate between two different states, such as normal versus abnormal, but yield as their result a grading on a scale with more than two grading levels, ROC analysis provides corresponding values of true positive (sensitivity) and false positive (1 − specificity) fractions for different levels of a decision threshold. Accordingly, variations of the threshold value at the output unit that discriminate between normal and abnormal patterns yielded four pairs of sensitivity/specificity values for each network instance. These data were used to derive five individual and one average ROC curve by computer analysis using the computer program ROCFIT (*22*).

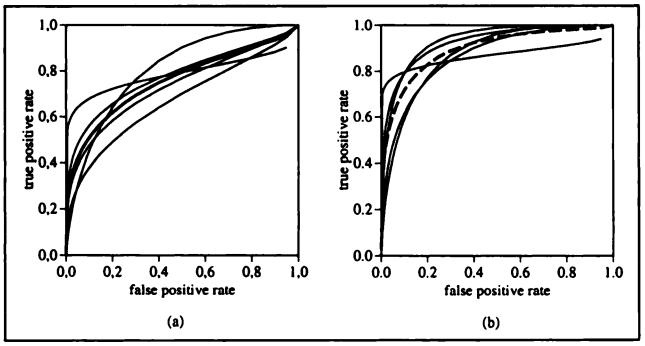

FIGURE 3. ROC curves obtained from five instances of artificial neural networks to detect significant CAD with (a) angiography and (b) the expert human reading as the reference standards. Individual curves = thin lines; average curves = bold lines.

For the assessment of the severity of CAD, five instances of a network topology with two output units (O_1 and O_2) were trained to classify segmental thallium uptake into three patterns: normal [0 0], single-territory disease [1 0] and multiple-territory disease [0 1] or [1 1]. Networks were again trained using either results from coronary angiography or an expert reading as reference standards. A 3 × 3 classification matrix was obtained for each network during evaluation, and these matrices were then summed into a lumped evaluation matrix.

Similarly, five instances of a neural network with two output units were trained to assess the localization of significant CAD by differentiating between two vascular territories assigned to the vascular beds of the LAD and the CX/RCA, as indicated previously. Diagnostic performance was assessed by generating average values of positive and negative predictive accuracies for each vascular territory.

RESULTS

Detection of Significant CAD

Figure 3 displays individual and an average ROC curve obtained from five different artificial neural networks trained for the detection of significant CAD with coronary angiography (Fig. 3a) or human expert readings (Fig. 3b) as reference standards. The observed variation between different ROC curves attests to the influence that the selection of training sets may exert on the performance of artificial neural networks.

The two average ROC curves that describe the average diagnostic performance of artificial neural networks are depicted in Figure 4 together with the ROC curve that is obtained when the expert reading was compared with coronary angiography. At a specificity of 90%, the average sensitivity of the network was 51% compared with angiography and 72% compared with the human expert. In comparison, the corresponding sensitivity for the human expert with angiography as the reference standard was 86%. At a sensitivity of 90%, the average specificity of the network was 20% when angiography and 70% when expert readings were taken as reference standards. In comparison, the specificity for the detection of CAD of the human expert was 87% at a sensitivity of 90%. Thus, compared with angiography, the human expert, who based his assessment

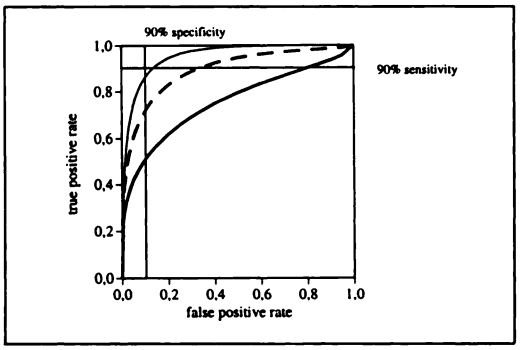

FIGURE 4. Comparison of ROC curves for the detection of significant CAD: human expert versus angiography (thin line), average neural network versus human expert (broken thick line) and average neural network versus angiography (solid thick line).

not only on segmental thallium uptake values but also on the scintigraphic images, demonstrated a better diagnostic accuracy than did the artificial neural networks.

Assessment of Severity of CAD

Figures 5a and b depict graphic representations of the 3 × 3 crosstabulation matrices that are generated when test cases are classified by neural networks into patterns reflecting normal, single-territory and multiple-territory disease, which are compared with angiography (Fig. 5a) or human expert readings (Fig. 5b). The average concordancy rate derived from five network instances was 40% for angiography and 56% for the human expert as reference standards. When expert readings were compared with angiography (Fig. 5c), the concordancy rate was 58%.

For normal cases, as defined by the reference methods, the networks correctly recognized a normal pattern in 56% (angiography) and 69% (human expert). For cases defined as multiple-territory disease, neural networks were able to associate an abnormal pattern (single or multiterritory disease) in 77% (angiography) and 86% (human expert). For cases with single-territory disease, the networks discerned an abnormal pattern in 73% (angiography) and 70% (human expert). Among abnormal cases, the differentiation between single- and multiple-territory disease was better when the human expert rather than angiography was taken as reference standard.

Assessment of Localization of CAD

Figures 6a and b display negative and positive predictive accuracies obtained from artificial neural networks for the assessment of localization of CAD in the LAD and the CX/RCA vascular territories in comparison to angiography (Fig. 6a) and the human expert reading (Fig. 6b). For both territories, positive predictive accuracies for the detection of significant CAD did not vary noticeably between networks and ranged from 79% to 86%. For negative predictive accuracies, the values were better when they were compared with the human expert (70% for the LAD and 68% for the CX/RCA territory) than with angiography (52% for the LAD and 60% for the CX/RCA territory). Figure 6c shows positive and negative predictive accuracies when

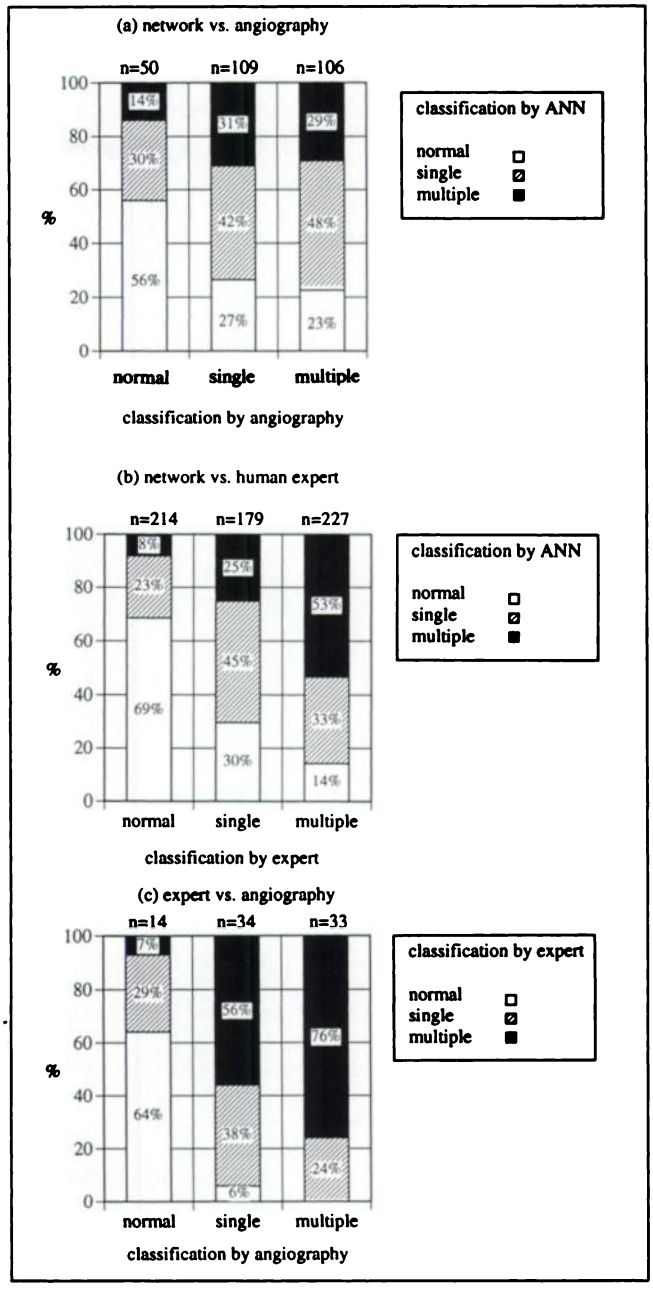

FIGURE 5. Comparison between classifications of CAD into three patterns concerning the severity of disease: normal, single-territory disease and multiple-territory disease. (a) Neural network versus angiography. (b) Neural network versus human expert. (c) Human expert versus angiography. For artificial neural networks (ANN), the number of cases (n) refers to the summed results involving five different network instances.

the human expert was compared with angiography. Although the positive predictive accuracies were comparable to the values that were obtained from the neural networks, negative predictive accuracies were higher.

DISCUSSION

This study used artificial neural networks to generate an automated computer-based assessment concerning the presence, severity and localization of significant CAD from

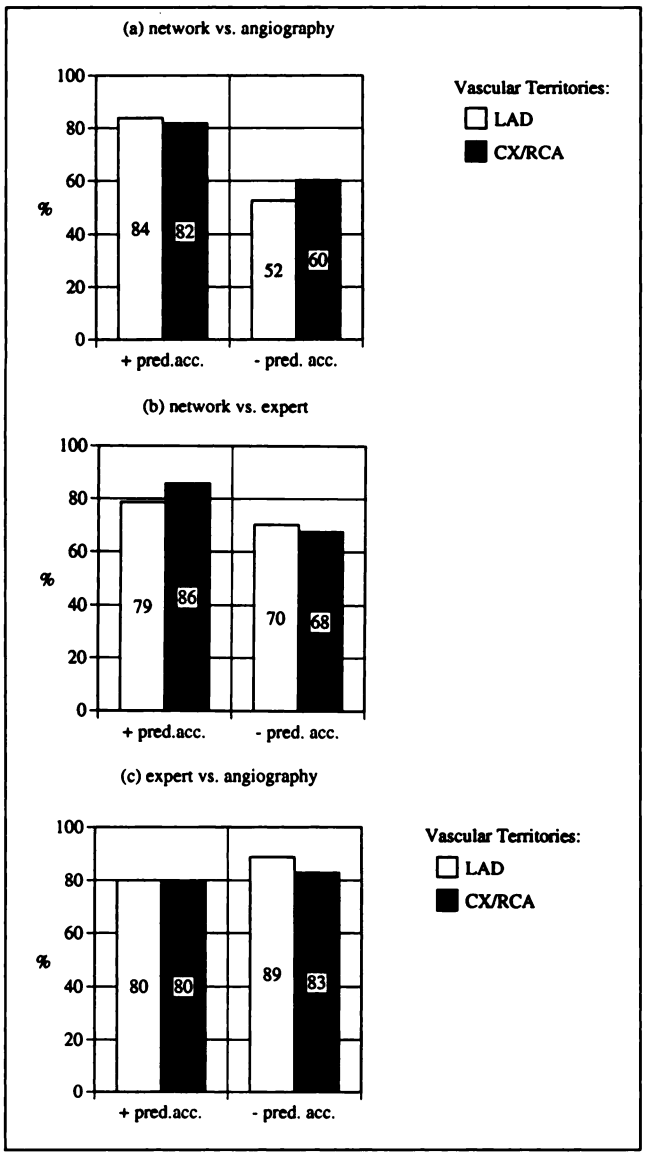

FIGURE 6. Comparison of positive and negative predictive accuracies concerning the presence of significant CAD in two vascular territories subtended by the left anterior descending artery (LAD) and by the left circumflex and right coronary artery (CX/RCA). (a) Neural network versus angiography. (b) Neural network versus human expert. (c) Human expert versus angiography.

relative segmental thallium uptake values of planar dipyridamole stress/redistribution scintigrams. Different network configurations were developed and evaluated against results from coronary angiography and from the visual interpretation by an expert reader.

The diagnostic performance of neural networks was better when the results from the human expert reading rather than those from angiography were taken as the reference standard. Although coronary angiography is based on morphologic criteria to assess the presence, severity and localization of CAD, myocardial scintigraphy depends on differences in the relative myocardial perfusion to assess CAD and may better reflect the hemodynamic significance of luminal obstructions in coronary arteries. Accordingly, neural networks that are trained to simulate the human expert are expected to exhibit better diagnostic performance than when they are trained to predict angiographic results. Moreover, angiographic results were available in only 81 of 159 patients, so that the size of training and evaluation sets for angiographic results as the reference method were limited. Especially for the diagnostic task to differentiate between three patterns of severity of CAD (normal, single territory and multiple territory), the small number of training cases for each diagnostic category may have been insufficient to serve as a representative sample set. Therefore, differences between training and evaluation sets, especially concerning the number of included cases, may also explain why neural networks performed worse when angiographic results were predicted rather than human expert readings.

The diagnostic accuracy of thallium scintigraphy depends on the prevalence and severity of CAD in the study population (*3*). The inclusion of patients with prior transmural myocardial infarction, as in this study population, may especially affect the sensitivity and specificity of thallium scintigraphy. To assess the influence of the study population on diagnostic accuracy, the authors also compared for each diagnostic task the human expert readings with the results from angiography. It was found that in the subgroup of 81 patients who underwent angiography, the human expert performed consistently better than did artificial neural networks. Although this difference in diagnostic performance may be attributed to the method, it potentially could also imply that the information content of the 45 integer numbers that result from segmental analysis is considerably less than the information that is present in the scintigraphic images, which were used by the human expert to derive his diagnostic classifications. Thus, artificial neural networks that use entire images as the input pattern may possibly achieve a better diagnostic performance.

The present study was based on planar thallium scintigrams rather than thallium SPECT images. Although SPECT imaging is considered the state-of-the-art imaging technique, offering an improved contrast resolution, planar thallium imaging still is commonly used in clinical routine because it is technically and financially less demanding and has a long record of proved clinical utility. However, the limited ability of planar imaging to discern anatomic segments may also affect the diagnostic accuracy of automated image interpretation systems. In a previous study, Fujita et al. (*15*) reported that neural networks may be useful to interpret polar map displays generated from SPECT images. However, as the evaluation set with 16 cases was small, a comprehensive evaluation regarding the diagnostic performance of their neural network could not be conducted. Compared with human observers, the artificial neural network appeared to perform better than a resident but worse than experienced radiologists. The results of Fujita et al. (*15*) suggest that an automated interpretation of myocardial perfusion scintigrams by neural

networks may perform better when tomographic rather than planar images are used because of the improved contrast resolution of SPECT images.

An inherent limitation of artificial neural networks is their associated level of incompetence. For example, networks, as presented in this study, generate output patterns for any set of 45 input numbers regardless of whether these originate from a thallium scintigraphy or are chosen at random. In contrast, rule-based expert systems usually provide no output if they are provided with inadequate or inconsistent input information. Hybrid systems that combine features from both rule-based systems and artificial neural networks might overcome the limitations of either approach.

In conclusion, this study demonstrated that artificial neural networks offer a novel and promising approach to develop computer-based systems for an automated interpretation of ^{201}Tl scintigrams. However, to achieve a level of diagnostic accuracy that may be acceptable for clinical applications, artificial neural networks need to be trained with sufficiently large sets of training cases. Further studies are required to delineate more precisely the merits and limitations of artificial neural networks for an automated interpretation of myocardial perfusion scintigrams.

ACKNOWLEDGMENTS

Charles Metz, PhD, Department of Radiology, University of Chicago, provided the computer programs for the ROC analysis. The technical assistance of Brigitte Slama and Regina Wagner is gratefully acknowledged. This work was supported in part by a research grant from Informatica GesmbH., Vienna, Austria.

REFERENCES

1. Sochor H, Pachinger O, Ogris E, Probst P, Kaindl F. Radionuclide imaging after coronary vasodilation: Myocardial scintigraphy with thallium-201 and radionuclide angiography after administration of dipyridamole. *Eur Heart J* 1984;5:500–509.
2. Leppo JA. Dipyridamole-thallium imaging: the lazy man's stress test. *J Nucl Med* 1989;30:281–287.
3. Kaul S. A look at 15 years of planar thallium-201 imaging. *Am Heart J* 1989;118:581–601.
4. Leppo J, O'Brien J, Rothlendler JA. Dipyridamole-thallium-201 scintigraphy in the prediction of future cardiac events after acute myocardial infarction. *N Engl J Med* 1984;310:1014–1018.
5. Hendel RC, Layden JJ, Leppo JA. Prognostic value of dipyridamole thallium scintigraphy for evaluation of ischemic heart disease. *J Am Coll Cardiol* 1990;15:109–116.
6. Burow RD, Pond M, Schafer W, Becker L. "Circumferential profiles": a new method for computer analysis of thallium-201 myocardial perfusion images. *J Nucl Med* 1979;20:771–777.
7. Okada RD, Boucher CA, Kirshenbaum HK, et al. Improved diagnostic accuracy of thallium-201 stress test using multiple observers and criteria derived from interobserver analysis of variance. *Am J Cardiol* 1980;46:619–624.
8. Rigo P, Bailey IK, Griffth LSC, et al. Value and limitations of segmental analysis of stress thallium myocardial imaging for localization of coronary artery disease. *Circulation* 1980;61:973–981.
9. Maddahi J, Garcia EV, Berman DS, et al. Improved noninvasive assessment of coronary artery disease by quantitative analysis of regional stress myocardial distribution and washout of thallium-201. *Circulation* 1981;64:924–935.
10. Winston PH. *Artificial intelligence*, 2nd edition. Reading, MA: Addison-Wesley; 1984.
11. Ezquerra NF, Shapiro S, Garcia EV, DePuey EG, Hise HL. A knowledge-based system for interpreting cardiovascular nuclear medicine images. In: *Computers in cardiology 1986*. New York: IEEE Computer Society; 1987.
12. Depuey EG, Garcia EV, Ezquerra NF. Three-dimensional techniques and artificial intelligence in thallium-201 cardiac imaging. *AJR Am J Roentgenol* 1989;152:1161–1168.
13. Porenta G, Dorffner G, Schedlmayer J, Sochor H. Parallel distributed processing as a decision support approach in the analysis of thallium scintigrams. In: Ripley KL, Murray A, eds. *Computers in cardiology 1988*. New York: IEEE Computer Society; 1989.
14. Reiber JHC, Bloom G, Wiezer B, et al. ESATS, an expert system for the quantitative analysis of thallium-201 scintigrams. In: Ripley KL, Murray A, eds. *Computers in cardiology 1988*. New York: IEEE Computer Society; 1989.
15. Fujita H, Katafuchi T, Uehara T, Nishimura T. Application of artificial neural network to computer-aided diagnosis of coronary artery disease in myocardial SPECT bull's-eye images. *J Nucl Med* 1992;33:272–276.
16. Fintel DJ, Links JM, Brinker JA, et al. Improved diagnostic performance of exercise thallium-201 single photon emission computed tomography over planar imaging in the diagnosis of coronary artery disease: a receiver operating characteristic analysis. *J Am Coll Cardiol* 1989;13:600–612.
17. Rumelhart DE, McClelland JL. *Parallel distributed processing, explorations in the microstructure of cognition*, Vol. 1. Cambridge, MA: A Bradford Book; 1986.
18. McClelland JL, Rumelhart DE. *Parallel distributed processing, explorations in the microstructure of cognition*, Vol. 2. Cambridge, MA: A Bradford Book; 1986.
19. Maren AJ, Harston CT, Pap RM. *Handbook of neural computing applications*. San Diego: Academic Press; 1990.
20. Linhart G, Dorffner G. *Handbuch VieNet2*. Technical report 93-13. Austrian Research Institute of Artificial Intelligence; 1993.
21. Metz CE. Basic principles of ROC analysis. *Semin Nucl Med* 1978;8:283–298.
22. Metz CE, Shen JH, Wang PL, Kronman HB, Herman BA. *ROCFIT (Apple Macintosh version)*. Chicago: Department of Radiology, University of Chicago; 1991.